ACS OMEGA

http://pubs.acs.org/journal/acsodf

Article

# Biosynthesis and Optimization of ZnO Nanoparticles Using *Ocimum lamifolium* Leaf Extract for Electrochemical Sensor and Antibacterial Activity

Eneyew Tilahun, Yeshaneh Adimasu, and Yilkal Dessie*

Cite This: *ACS Omega* 2023, 8, 27344−27354

Read Online

ACCESS | Metrics & More | Article Recommendations

**ABSTRACT:** In this study, zinc oxide nanoparticles (ZnO NPs) were synthesized using an aqueous extract of the *Ocimum lamifolium* (*O. lamifolium*) plant. The I-optimal coordinate exchange randomized response surface methodology (RSM) was used to optimize the effect of the zinc acetate precursor, temperature, and time on ZnO NPs by designing nine runs. From ANOVA analysis, the significance and validity of the designed model showed that the optimal values of the zinc acetate precursor, temperature, and time during ZnO NPs synthesis were found to be ∼0.06 M, ∼30 °C, and ∼1.35 h, respectively. The obtained ZnO NPs under these optimized conditions were characterized and explored by UV−vis, TGA/DTA, FTIR, XRD, SEM-EDX, TEM, HRTEM, and SAED. Furthermore, the electrocatalytic performance of ZnO NPs was performed for sulfamethoxazole (SMZ) sensing activity with a 0.3528 $\mu$M (S/N = 3) limit of detection (LOD). In addition, an antibacterial study revealed that ZnO NPs confirmed an excellent zone of inhibition against *E. coli*, *S. aureus*, *P. aeruginosa*, and *S. pyogen* pathogenic drug resistance bacterial strains at concentrations of 50, 75, and 100 $\mu$g/mL. Thus, ZnO NPs synthesized using the *O. lamifolium* leaf have a potential electrocatalytic activity for diverse organic pollutant detection as well as a desirable material for such drug resistance antimicrobial strains.

## 1. INTRODUCTION

Nanoparticles (NPs) in nanotechnology areas have particular interest in creating unique and new nanoscale (1−100 nm) materials for a wide range of applications.[1] The small particle size that is found in the nanomaterial size range shows a tremendous increase in specific surface area with low dimensions, which results in a wider range and efficient application in a variety of fields.[2] Among semiconducting nanometal oxide-based materials are zinc oxide (ZnO) NPs, which are some of the most effective transition metal oxides that exhibit high antibacterial activity[3] and have been widely used for the detection and quantification of toxic molecules found within different components, such as drugs, foods, drinking matter, soaps, and many others.[4] This is due to their low cost, nontoxicity to eukaryotic cells at therapeutic dosages, low electric resistance, good stability, high catalytic efficiency, high UV protection, excellent electron transfer capability, and, at the same time, biocompatibility properties.[5−7]

In terms of antibacterial activity, ZnO NPs have been used for food safety, as they can protect agricultural crops and products from food-borne-related pathogens. This application was successful due to the nontoxicity and decreasing particle size nature of ZnO NPs.[8] For example, Fatimah et al. have reported 2.714 and 4.694 nm sized ZnO NPs using *Mimosa pudica* and coffee powder extracts, respectively.[9] Later, Doan Thi et al. reported microstructural ZnO NPs synthesized using orange fruit peel extract, and the NPs had strong antibacterial activity toward *Escherichia coli* (*E. coli*) and *Staphylococcus aureus* (*S. aureus*) without UV illumination at an NP concentration of 0.025 mg/mL after 8 h of incubation.[10] On the other hand, due to their good stability, selectivity, antijamming ability, and reproducibility, ZnO NPs could possess excellent electrocatalytic behavior for sensor applications.[11] Especially the green nanomodified carbon paste working electrode strategy has been given a lot of attention due to its novel and cost-effectiveness techniques.[12] Patil et al. have reported the detection of trimethoprim (TMP) using a nanostructured ZnO NP-modified carbon paste electrode with an anionic surfactant and sodium dodecyl sulfate (SDS) with the help of voltametric techniques. The electrode process of TMP was irreversible and diffusion controlled with two electrons transferred. The effective concentration range ($8.0 \times 10^{-7}$ M to $1.0 \times 10^{-5}$ M) of TMP was obtained by varying the concentration, with a lower limit of detection obtained of $2.58 \times 10^{-8}$ M.[13] However, the low sensitivity and inefficient antibacterial activity found in biological and pharmaceutical samples have not yet been solved and are still a challenge in large-scale applications due to several factors. Those factors are the synthesis methods, optimization techniques, and particle sizes. Therefore, in this study, all factors are effectively improved to increase the electrochemical sensor and antibacterial activity.

**Received:** April 20, 2023
**Accepted:** July 11, 2023
**Published:** July 24, 2023

Scheme 1. Schematic Diagram of Green Synthesis Mechanism of ZnO NPs Using *O. lamifolium*

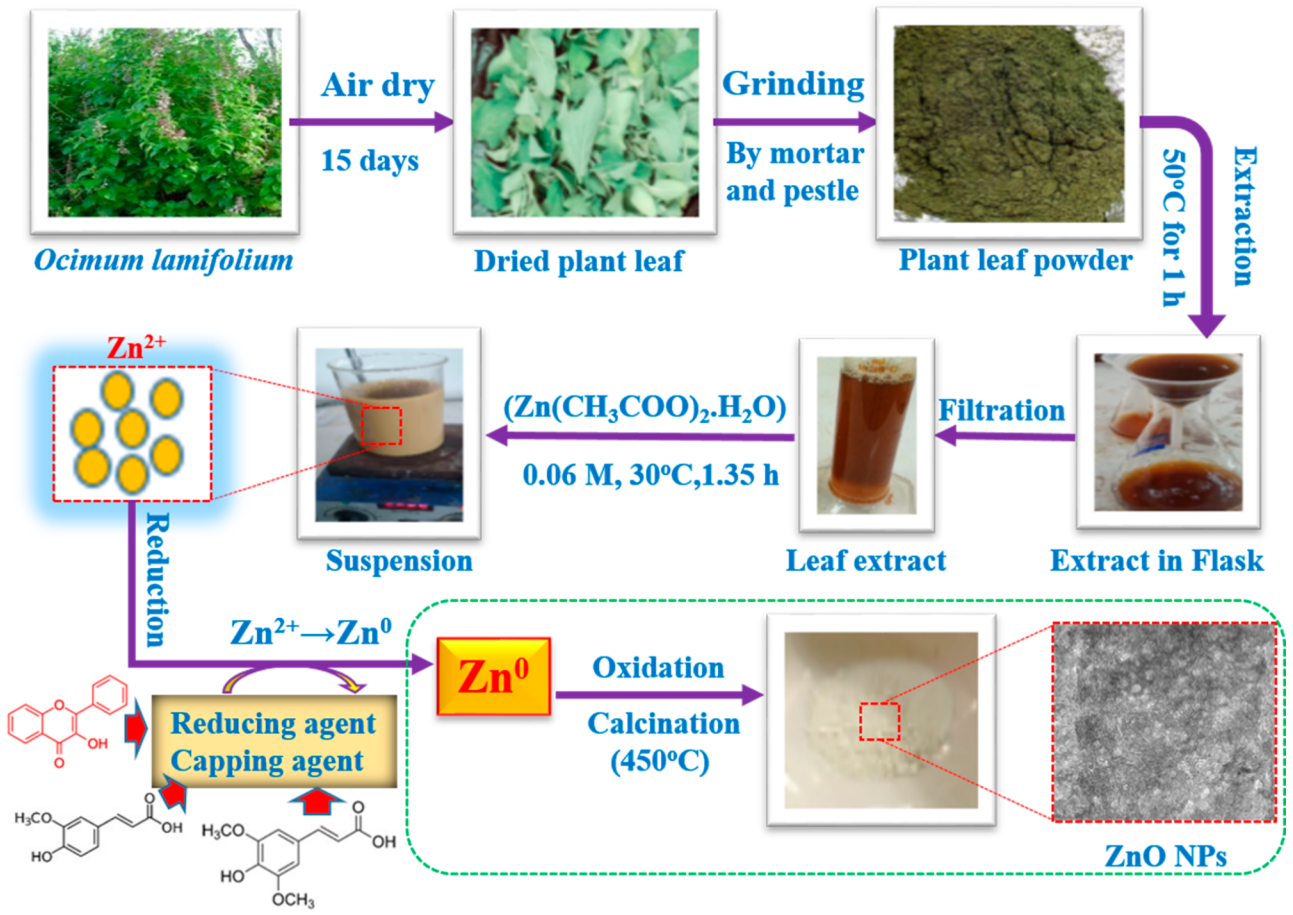


Recently, green synthesis of ZnO NPs has gained much attention in nanoscience and nanoengineering technology due to their cost-effectiveness, reliability, environmental friendliness, and use of cheap instruments during their synthesis.[14−17] Principally, different sources of plants and their various components produce active natural molecules like phenols, flavonoid polyphenolics, and alkaloids that can act as a good reducing and stabilizing agents for efficient ZnO NP preparation.[18−21] Previously, different plants, such as *Myristica fragrans*,[22] *Lawsonia inermis*,[23] *Pelargonium odoratissimum* (L.),[24] *Hagenia abyssinica*,[25] *Calotropis gigantean*,[26] orange fruit peel,[10] *Ananas comosus* fruit,[27] *Cocos nucifera* leaf,[28] and *Catharanthus roseus* leaf,[29] have been reported to synthesize ZnO NPs. However, until now, all of the green synthesis processes of ZnO NPs have not been optimized properly, which reduces their effectiveness. Hence, in this study, to improve such a problem, an efficient, recent, and cost-effective mathematical and statistical analysis method known as response surface methodology (RSM) improves and solves all of the demerits that were identified in classical methods. RSM is a very popular experimental design to reduce the cost and time. It has been widely applied to get the optimum conditions during well-dispersed and stabilized NP synthesis, followed by evaluating interaction effects between each experimental variable.[30]

In this study, ZnO NPs were synthesized using *Ocimum lamifolium* (*O. lamifolium*) leaf extract and optimized with randomized RSM; I-optimal coordinate exchange; and quadratic study type, design type, and Design Model. After optimization, the obtained green ZnO NP characterization and electrochemical detection of sulfamethoxazole (SMZ) as well as antibacterial activity toward *Eschricha coli* (*E. coli*), *Staphylococcus aureus* (*S. aureus*), *Pseudomonas aeruginosa* (*P. aeruginosa*), and *Streptococcus pyogenes* (*S. pyogen*) were reported.

## 2. EXPERIMENTAL SECTION

**2.1. Chemicals and Reagents.** Hydrated zinc acetate ($Zn(CH_3COO)_2{\cdot}H_2O$), sodium hydroxide (NaOH), potassium hydroxide (KOH), sulfamethoxazole ($C_{10}H_{11}N_3O_3S$), and ethanol ($CH_3CH_2OH$) were purchased from Sigma-Aldrich. Distilled water (DW) was used to prepare all of the solutions. All of the chemicals and reagents were of analytical grade and used as received without further purification.

**2.2. *Ocimum lamifolium* Leaf Extract Preparation.** A leaf of *O. lamifolium* was collected from Adama Science and Technology University, Ethiopia. The collected leaves were washed with DW to remove dust particles and impurities from the surface of the plant leaf. Then, the leaf was allowed to shed until completely dry at room temperature for 2 weeks. After drying, the leaf was crushed by grinding in a mortar and pestle for the formation of a homogeneous powder mixture. Afterward, 10 g of dried powder of *O. lamifolium* was added to a 500 mL Erlenmeyer flask, and the flask was filled with 400 mL of DW. The mixed components were then heated to 50 °C followed by stirring for 1 h. After cooling, the solution was filtered with Whatman no. 1 filter paper, and the extract was


https://doi.org/10.1021/acsomega.3c02709
ACS Omega 2023, 8, 27344−27354

Table 1. Design of the Model

| factor | name | units | type | subtype | coded min | coded max | mean | std. dev. |
|---|---|---|---|---|---|---|---|---|
| A | zinc acetate | mM | numeric | discrete | −1.000 = 0.01 | 1.000 = 0.1 | 0.0533333 | 0.0390512 |
| B | temperature | °C | numeric | discrete | −1.000 = 30 | 1.000 = 90 | 60 | 25.9808 |
| C | time | h | numeric | discrete | −1.000 = 1 | 1.000 = 2 | 1.5 | 0.433013 |

collected in a colored bottle before being placed in the refrigerator at 4 °C for further use.

**2.3. Biosynthesis of ZnO NPs.** The biosynthesis of ZnO NPs was synthesized by following the literature with modifications.[30] Briefly, aqueous solutions of zinc acetate (0.01, 0.05, and 0.1 M) were prepared. Nine runs with three factors and three levels were designed by using Design-Expert 10 software. So, to synthesize ZnO NPs, the three aqueous solutions of zinc acetate were mixed with 20 mL of *O. lamifolium* leaf extract. The mixtures were allowed to stand for 1, 1.5, and 2 h at a temperature of 30, 60, and 90 °C. The pH of each of the formed suspensions was adjusted to pH 12 using 0.1 M NaOH solution as a precipitating agent. The formed suspension was placed in a refrigerator overnight. Then, the precipitate was centrifuged at 3000 rpm for 10 min in three consecutive steps using ethanol, DW, and ethanol, respectively. Finally, the optimized washed sample was oven-dried, and after TGA confirmation, the sample was calcined at 450 °C. The detailed green synthesis mechanism of the ZnO NPs is summarized in Scheme 1.

**2.4. Statistical Analysis.** I-optimal coordinate exchange randomized RSM was used to optimize experimental factors in the preparation of ZnO NPs. The three experimental factors, zinc acetate concentration, temperature, and time, were studied very well, as shown in Table 1, to find their influences on the prepared NPs. In order to illustrate the validity of the designed model, ANOVA, correlation coefficients ($R^2$), and probability ($p$ value < 0.05) were studied. In addition, the adequacy, precision, and significance of the model were studied to ensure its adequacy.

**2.5. Characterization of ZnO NPs.** The synthesis of ZnO NPs was elucidated by a UV−vis spectrophotometer in the range of 200−800 nm (UV−vis 1800-double beam spectrophotometer, Shimadzu, Japan). Thermogravimetric-differential thermal analysis (TGA-DTA) was carried out on a DTG-60H detector (Shimadzu, Japan) under $N_2$ gas. Fourier transform infrared spectroscopy (FTIR, PerkinElmer 65, PerkinElmer, Inc., Waltham, USA) was performed in the range of 4000−400 $cm^{-1}$. Crystallite size determination of ZnO NPs was done by using an X-ray diffractometer (XRD-7000, Shimadzu, Tokyo, Japan) with a voltage of 40 kV and a current of 30 MA with Cu K = 1.5406 radiation as an X-ray source at a 10−80° diffraction angle. The surface morphology and chemical composition of prepared ZnO NPs were explored using a scanning electron microscope and energy dispersive X-ray spectroscopy (SEM-EDX-EVO 18 model-low vacuum facility-ALTO 1000 Cryo attachment), respectively. The microstructural morphology, crystalline size distribution, and purity of the synthesized NPs were elucidated using TEM, HRTEM, and SAED micrographs using the JEOL TEM 2100 HRTEM machine, and all image analyses were done by Gatan and ImageJ Software. Finally, the electrochemical property of the ZnO NPs modified carbon paste electrode (CPE) as a working electrode was investigated using an electrochemical workstation, Model CHI608E (CH Instruments, Inc. Austin, TX, USA), with 1 M KOH solution as an electrolyte. Ag/AgCl/KCl (0.1 M) and platinum wire were used as reference and counter electrodes, respectively. A modification of the working electrode (ZnO/CPE) was prepared by following the procedure from our previous work.[12]

**2.6. Screening of Antibacterial Activity.** The antibacterial activity of ZnO NPs was tested against *E. coli*, *S. aureus*, *P. aeruginosa*, and *S. pyogen* pathogenic bacteria using a disc diffusion method.[30] The standard culture of test bacteria was first spread onto the surface of Mueller Hinton agar plates. Since, Mueller Hinton agar medium was adjusted to neutral pH with 1 M NaOH and DW to form a 1 L solution, four wells were made in each plate and were filled with ZnO NPs at concentrations of 50, 75, and 100 $\mu$g/mL with ampicillin as a positive control added to each plate. All of the plates were then covered with lids and incubated at 37 °C for 24 h. Finally, the size of inhibition zones was measured, and the antimicrobial activity of the ZnO NPs was expressed in terms of the average diameter of the inhibition zone in millimeters.

## 3. RESULTS AND DISCUSSION

**3.1. UV−Vis Spectral Analysis of Nine Experimental Runs.** The UV−vis absorption intensity is highly dependent on the concentration of ZnO NPs. From Figure 1, the increase

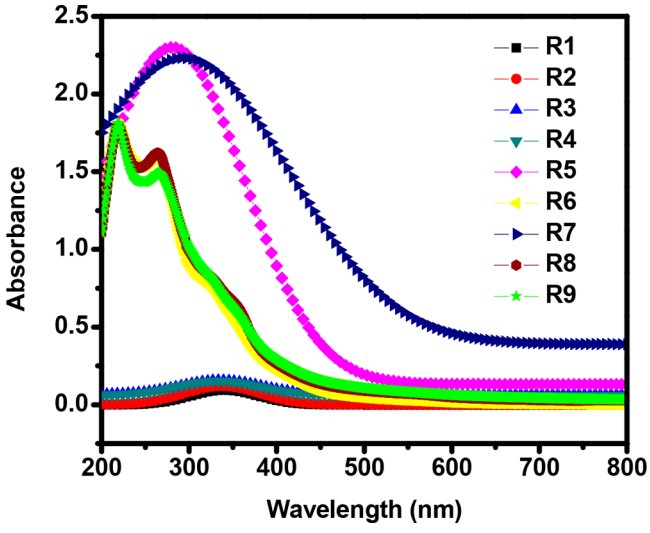


Figure 1. UV−vis spectra of biosynthesized ZnO NPs.

in intensity of ZnO NPs observed from each run indicated a better solubility and dispersion of ZnO NPs in solutions. Differences in wavelength positions indicated variations in morphology and size variations found in the prepared ZnO NPs, and the maximum absorption spectra in the range of 263−339 nm indicated the characteristic electron transitions from n → $\pi^*$ and $\pi \rightarrow \pi^*$. The actual maximal absorption of nine experimental runs and their predicted absorption maximum values are shown in Table 2.

From ANOVA analysis, the quadratic equation elucidated by I-optimal coordinate exchange confirmed that the model's $F$


https://doi.org/10.1021/acsomega.3c02709
ACS Omega 2023, 8, 27344−27354

**Table 2. Three Factor−Three Level Maximum Absorption Values Optimized by I-Optimal Coordinate Exchange Design Layout**

| | | factor 1 | factor 2 | factor 3 | response 1 absorption maximum (nm) | |
|---|---|---|---|---|---|---|
| std[a] | run | A: zinc acetate (mM) | B: temperature (°C) | C: time (h) | actual value | predicted value |
| 3 | 1 | 0.01 | 30 | 2 | 339.00 | 339.71 |
| 9 | 2 | 0.01 | 60 | 1.5 | 339.00 | 342.53 |
| 1 | 3 | 0.01 | 90 | 1 | 333.00 | 310.28 |
| 5 | 4 | 0.05 | 30 | 1.5 | 333.00 | 335.34 |
| 4 | 5 | 0.05 | 60 | 1 | 279.00 | 291.40 |
| 7 | 6 | 0.05 | 90 | 2 | 264.00 | 282.53 |
| 6 | 7 | 0.1 | 30 | 1 | 291.00 | 277.28 |
| 8 | 8 | 0.1 | 60 | 2 | 263.00 | 268.40 |
| 2 | 9 | 0.1 | 90 | 1.5 | 266.00 | 259.53 |

[a]std = standard deviation.

value of 10.67 implies the model is significant. Values of "Prob > *F*" less than 0.0500 indicate that model terms are significant. In this case, A and B are significant model terms. The "Pred R-Squared" of 0.5857 is in reasonable agreement with the "Adj R-Squared" of 0.7838; i.e., the difference is less than 0.2. "Adeq Precision" measures the signal-to-noise ratio. A ratio greater than 4 is desirable. From Table 3, the ratio of 7.747 indicates an adequate signal. This model can be used to navigate the design space. Hence, it is suggested that the experimental parameter with the highest *F* value from Table 3 is zinc acetate, and this parameter is the most influential factor that affects the synthesized NPs.

As shown in Figure 2, acetate concentration has the most positive effect on ZnO NPs. However, in all parameters, at higher values, their corresponding absorption maxima decrease (i.e., the synthesis of ZnO NPs is not effective). In addition, both temperature and reaction time have minor effects on the synthesis of ZnO NPs. According to Kahsay, the biosynthesis of ZnO NPs at low temperatures and for short periods of time does not affect the reaction.[30] From the development of ANOVA analysis, a quadratic polynomial model summarizes the influences of each experimental factor in terms of the codes in eqs 1 and 2, factors which show the sign and magnitude of each parameter.

$$\text{absorption maximum (nm)} = +299.62 - 31.22A - 20.56B - 11.69C \quad (1)$$

$$\text{absorption maximum (nm)} = +413.96346 - 693.71585 \times \text{zinc acetate} - 0.68542 \times \text{temperature} - 23.37500 \times \text{time} \quad (2)$$

From both equations, the relative impact of each experimental factor is identified from its parameter coefficients. Hence, the coefficients coded *A* corresponding to zinc acetate's actual values were higher compared to other coefficients. This indicates that the biosynthesis of ZnO NPs is highly influenced by the concentration of zinc acetate as compared with reaction temperature and time.

**3.2. Optimization of ZnO NPs.** The significant factors of zinc acetate, temperature, and time on the absorption maximum of ZnO NPs are shown in Figure 3. In Figure 3a−c, lower and intermediate amounts of zinc acetate, temperature, and time increase the synthesis of ZnO NPs, while higher values of all parameters are not effective for ZnO NP synthesis. As a result, the optimum conditions to synthesize ZnO NPs were found to be zinc acetate ≈ 0.06 M, temperature ≈ 30 °C, and time ≈ 1.35 h. Under these optimum conditions, the absorption maximum of ZnO NPs was 320.6 nm.

**3.3. Thermal, Optical, and XRD Analysis.** The TGA/DTA curves of the synthesized ZnO NPs were investigated to confirm their thermal stability and identify their calcination temperature, as shown in Figure 4a. Hence, the first weight loss occurred up to 200 °C because of the physical absorption of water molecules. The weight loss from 200 to 450 °C is due to the loss of binding water molecules. As can be depicted from the TGA/DTA spectra, beginning at 450 °C, no more weight loss is observed, which confirms that the green synthesized ZnO NPs are found to be thermally stable. Thus, the thermogram confirms that 450 °C is a suitable calcination temperature for the green ZnO NPs.

Figure 4b indicates the UV−visible absorption spectra of optimized ZnO NPs after calcination at 450 °C. Hence, its maximal absorption is found between 270 and 350 nm, and this confirms that this spectrum is truly validated as evidenced from I-optimal coordinate exchange randomized RSM. Therefore, this spectrum range indicated the clear synthesis of ZnO NPs. Figure 4b (inset) indicated a band-to-band transition pattern,[31] and the sharp nature of such a Tauc plot indicated the direct band gap nature of ZnO NPs with a value of ∼3.2 eV.

The FTIR spectra at about 3394 $cm^{-1}$ as shown in Figure 4c indicated the stretching and bending vibrations of the −OH and H−O−H groups of adsorbed water molecules, respectively. The absorption peak observed at about 2860−2919

**Table 3. ANOVA Analysis**

| source | sum of squares | degree of freedom | mean square | *F* value | *p* value Prob > *F* | model significances |
|---|---|---|---|---|---|---|
| model | 8266.34 | 3 | 2755.45 | 10.67 | 0.0130 | significant |
| A: zinc acetate | 5871.15 | 1 | 5871.15 | 22.73 | 0.0050 | |
| B: temperature | 2255.02 | 1 | 2255.02 | 8.73 | 0.0317 | |
| C: time | 728.52 | 1 | 728.52 | 2.82 | 0.1539 | |
| residual | 1291.22 | 5 | 258.24 | | | |
| Cor Total | 9557.56 | 8 | | | | |
| Adeq Precision | 7.747 | | | | | |
| R-Squared | 0.8649 | | | | | |
| Adj R-Squared | 0.7838 | | | | | |
| Pred R-Squared | 0.5857 | | | | | |



https://doi.org/10.1021/acsomega.3c02709
ACS Omega 2023, 8, 27344−27354

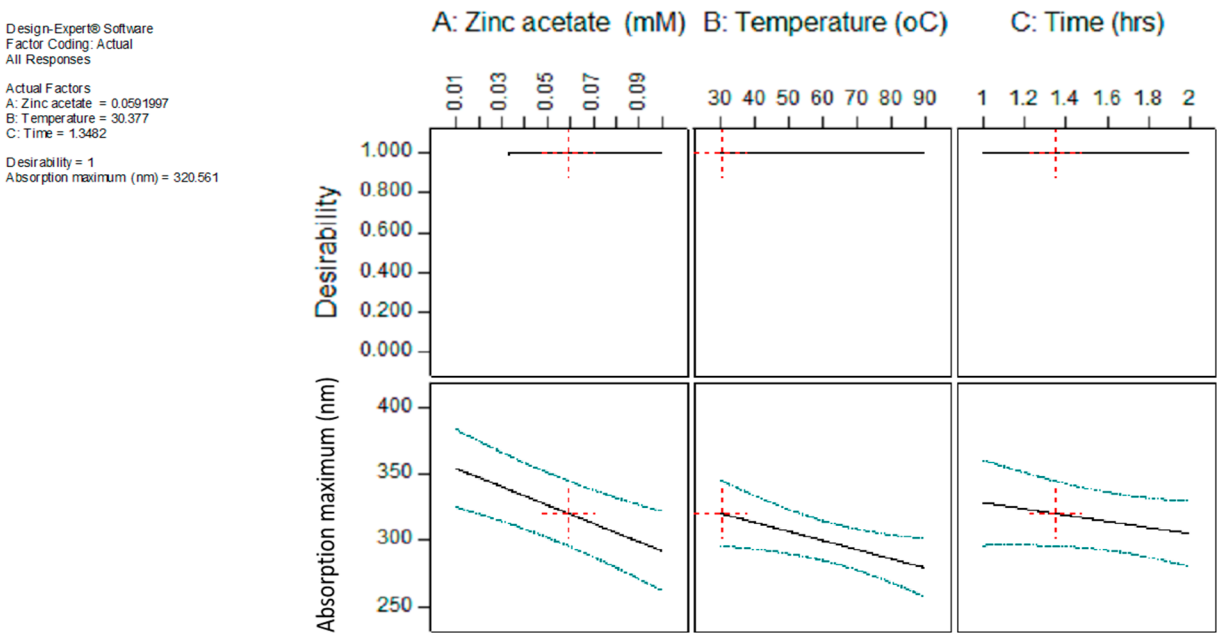


**Figure 2.** Effects of experimental factors on effective desirability.

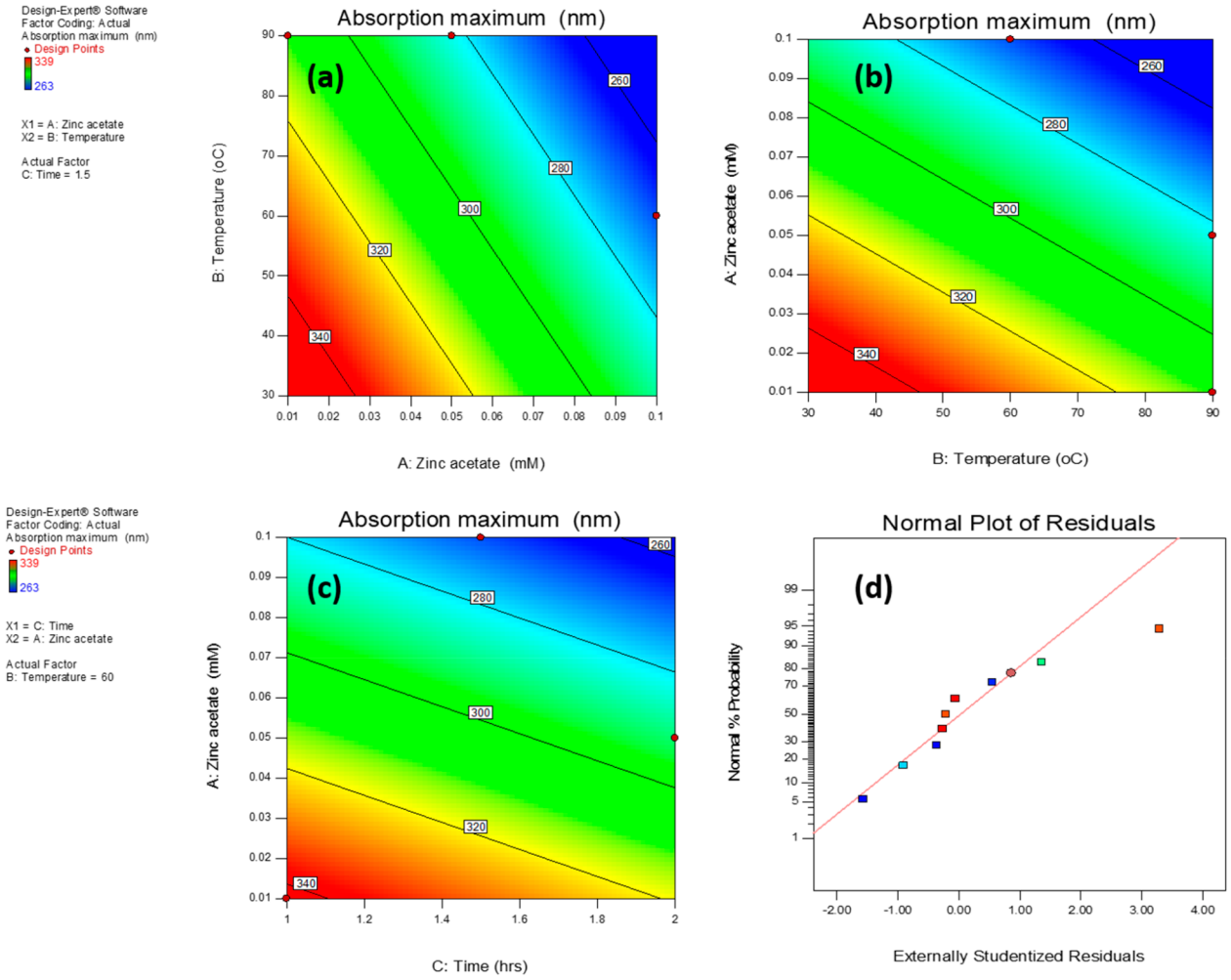


**Figure 3.** 2D plots of the effects of (a) zinc acetate and temperature, (b) temperature and zinc acetate, (c) zinc acetate and time, and (d) on absorption maximum and normal plot.



https://doi.org/10.1021/acsomega.3c02709
ACS Omega 2023, 8, 27344−27354

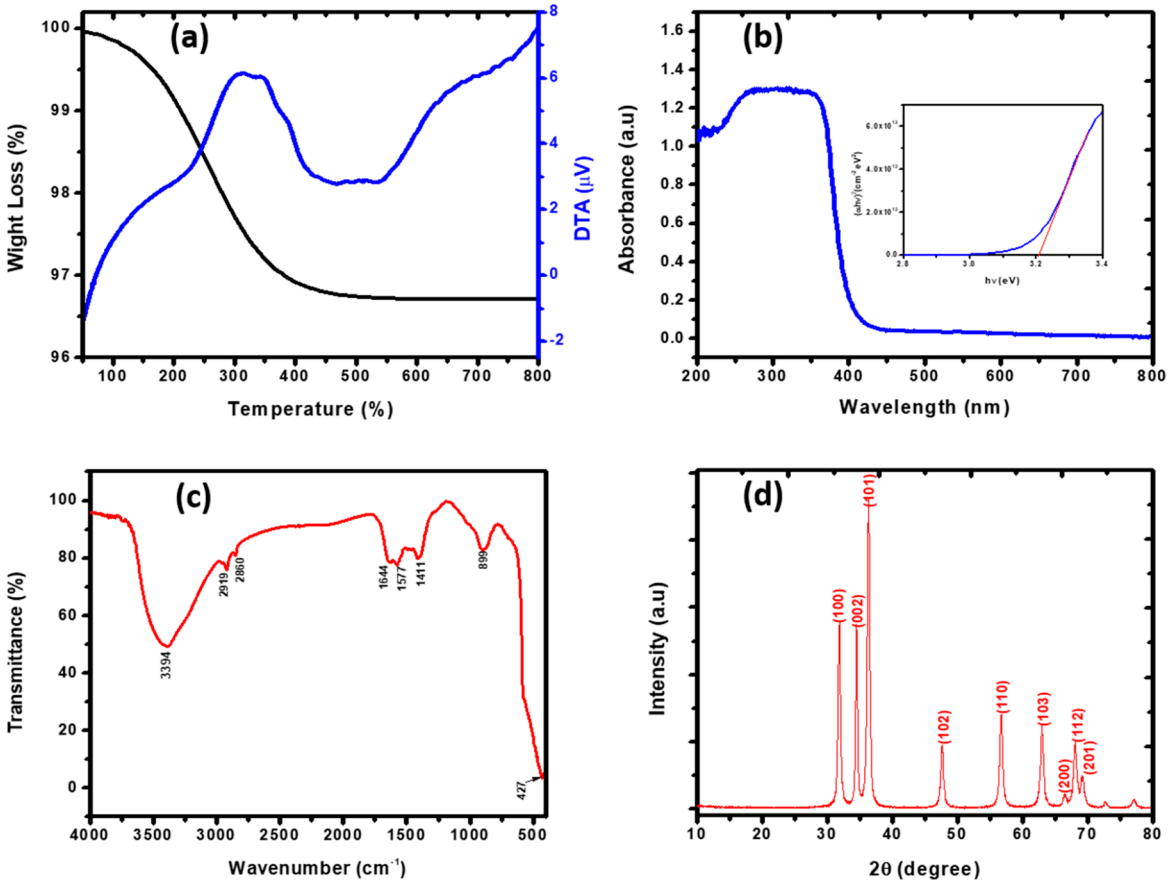


**Figure 4.** (a) TGA/DTA curves and (b) UV−vis spectra (inset: Tauc plot of ZnO NPs), (c) FTIR spectra, (d) XRD patterns of ZnO NPs.

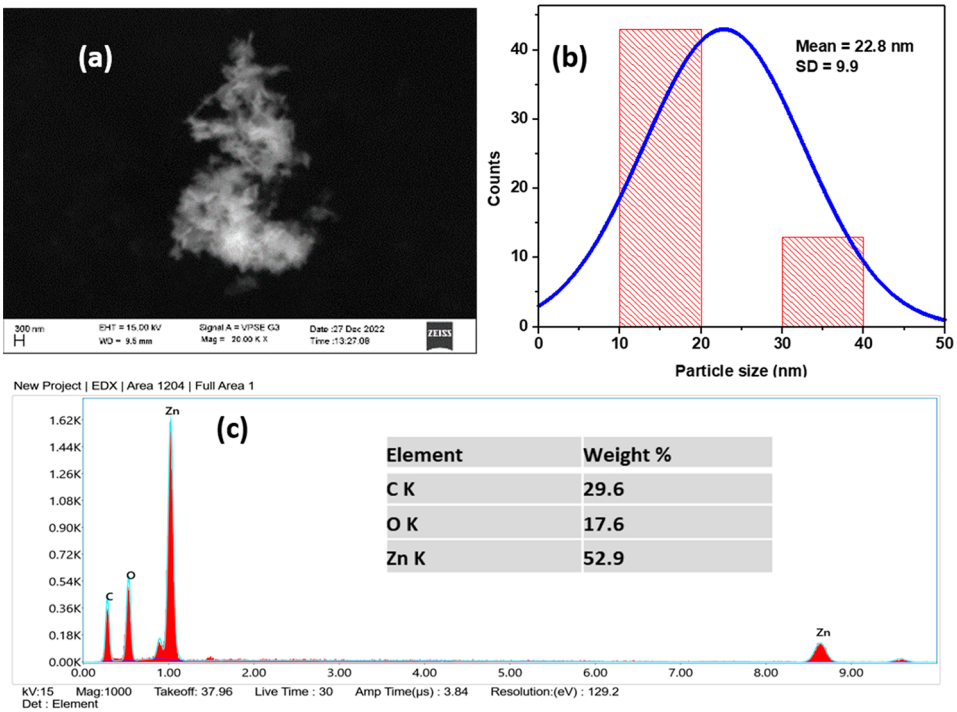


**Figure 5.** (a) SEM image, (b) average particle size, and (c) EDX spectrum of biosynthesized ZnO NPs.

$cm^{-1}$ indicated a C−H stretching vibration that might originate from binding plant phytochemicals of the aromatic of aldehyde.[32] The presence of such phytochemicals in the plant extract is responsible for reducing the metal ions into nanoscale materials.[33] On the other hand, the peak observed at 1411−1644 $cm^{-1}$ corresponds to the stretching vibration



https://doi.org/10.1021/acsomega.3c02709
ACS Omega 2023, 8, 27344−27354

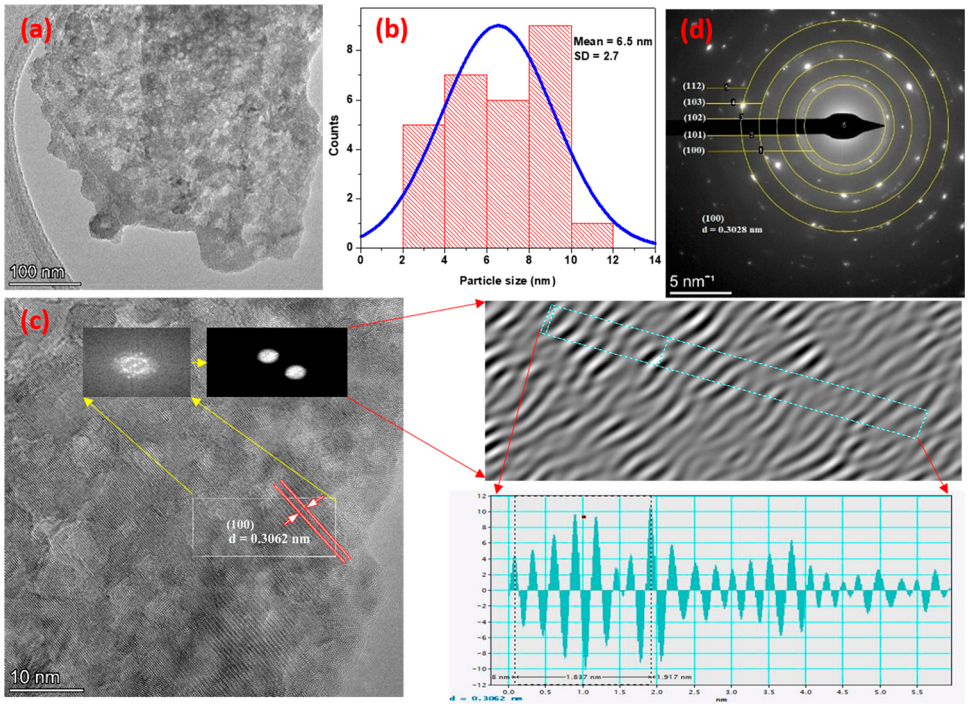


**Figure 6.** (a) TEM image, (b) particle size distribution, and (c) HRTEM and (d) SAED images.

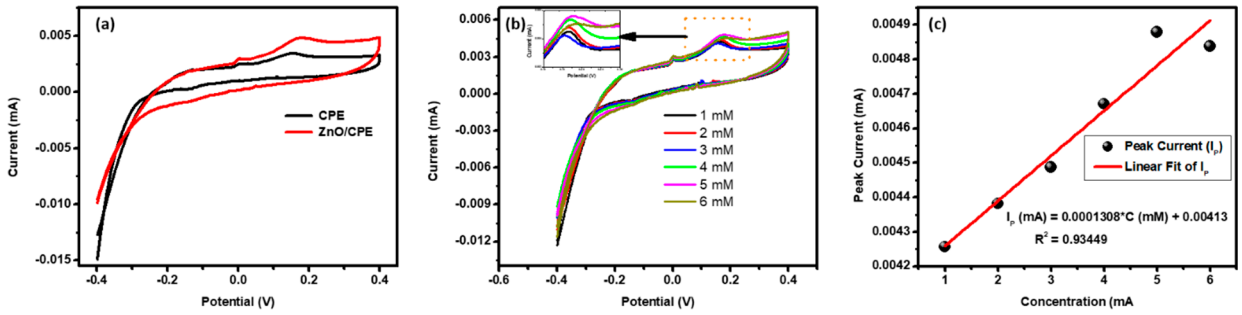


**Figure 7.** (a) CVs' response of bare CPE and ZnO/CPE toward 5 Mm SMZ, (b) CVs of different concentrations of SMZ using 1 M KOH solution as an electrolyte at ZnO/CPE, and (c) plot of peak current ($I_P$) versus concentration of SMZ at a scan rate of 50 mV $s^{-1}$.

characteristics of aromatic rings. The absorption peak found at 899 $cm^{-1}$ corresponds to the stretching of the C−H in-plane and out-of-plan bending. The peak observed at about 427 $cm^{-1}$ indicated the stretching of Zn−O vibrations.[25]

To evaluate the crystalline structure as well as the phase purity of the biosynthesized ZnO NPs, see Figure 4d. The XRD pattern showed a significant peak at 31.84° (100), 34.54° (002), 36.36° (101), 47.66° (102), 56.74° (110), 62.92° (103), 66.56° (200), 67.98° (112), and 69.22° (201). From the presented graph, it is observed that the biosynthesized nanomaterial has exactly matched the hexagonal phase/wurtzite structure ZnO NPs with JCPDS No. 00-036-1451.[34] The average crystallite size of the biosynthesized NPs was estimated by using Scherer's formula. In eq 3, $D$, $\lambda$, 0.9, and $\beta$ were the average crystallite size, wavelength (0.15416 nm), shape factor, and full width at half-maximum of peaks. Thus, the average ZnO NP crystallite size was calculated as 21.8 nm.

$$D = \frac{0.9\lambda}{\beta \cos \theta} \tag{3}$$

**3.4. SEM-EDX Analysis.** The surface morphology of aqueous *O. lamifolium* leaf extract ZnO NPs is investigated in Figure 5. Figure 5a, shows the SEM images of the distribution of nearly spherical ZnO NPs, and their average particle size is found to be 22.8 nm, as shown in Figure 5b. This size is comparable to the results that were elucidated by the XRD analysis. Figure 5c shows the EDX analysis, which confirmed the presence of Zn and O elemental signals in ZnO NPs. The presence of elemental carbon in the EDX result is a direct confirmation, as the biosynthesized material is obtained using plant leaf extract.

**3.5. TEM, HRTEM, and SAED Analysis.** The TEM images of the ZnO NPs are shown in Figure 6a. From the image, a spherical mesoparticle size distribution with an average size of 6.5 nm was elucidated from the histogram, as shown in Figure 6b. Hence, SEM and TEM analysis evidenced that the diameter of the NPs covered the range 6.5−22.8 nm. On the other hand, the HRTEM results shown in Figure 6c provide evidence that the structure of ZnO NPs and its *d*-spacing value at the (100) plane are fitted with XRD values. In addition, from Figure 6d, all planes evidenced from SAED also support the crystalline structure of the biosynthesized ZnO NPs as evidenced from the XRD spectra.



https://doi.org/10.1021/acsomega.3c02709
ACS Omega 2023, 8, 27344−27354

**3.6. Electrochemical Detection of SMZ.** The electrocatalytic activity of the ZnO NP-modified carbon paste electrode (CPE) as a working electrode was done in the presence of SMZ analyte, as shown in Figure 7a. It can be observed that the cyclic voltammograms (CVs) of bare CPE have not shown enough oxidation peak current, while ZnO modified CPE showed a clear oxidation peak of SMZ at about ~0.18 V. From this observation, it is elucidated that the prepared ZnO/CPE could be used as a better electrochemical sensor for SMZ. As a result, the better sensing activity on ZnO NPs modified with CPE is due to the improved intrinsic electrical conductivity of ZnO NPs.[35] Figure 7b shows the CV response of ZnO/CPE toward SMZ in the concentration range between 1 mM and 6 mM. The calibration plot shown in Figure 7c indicated good linear confirmation between the peak current and concentration of SMZ in the given range, with a regression coefficient ($R^2$) of 0.9345. Its limit of detection (LOD) was calculated by following the IUPAC method,[36] as shown in eq 4, with a value of 0.3528 $\mu$M.

$$\mathrm{LOD} = \frac{3\sigma}{m} \tag{4}$$

where $\sigma$ is the standard deviation of the blank ($1.54 \times 10^{-5}$) and $m$ is the slope of the calibration curve with a value of 1.31 $\times 10^{-4}$. In general, the LOD values of this work and previous work that was performed for SMZ detection by different working electrodes are shown in Table 4.

**Table 4. Summary of This Work and Previously Worked Linear Range and LOD Comparison for the SMZ Sensor**

| electrodes[a] | linear ranges ($\mu$M) | LOD ($\mu$M) | reference |
|---|---|---|---|
| g-$C_3N_4$/ZnO/GCE | 0.02−1105 | 0.0066 | 36 |
| GR/ZnO/GCE | 1−220 | 0.4 | 37 |
| ZnO@ZIF-8/CPE | 0.04−50 | 0.02 | 11 |
| 1M3OIMZTFB/NiO-NPs/CPE | 0.003−400 | 0.001 | 38 |
| MIP/BDD | 0.1−100 | 0.0241 | 39 |
| $Fe_3O_4$/ZIF-67/ILCPE | 0.01−520 | 0.005 | 40 |
| MWCNT/PBnc/SPE | 1−10 | 0.038 | 41 |
| MIP/Ppy/PGE | 25−750 | 35.9 | 42 |
| PPy/GC | 25−1250 | 1.03 | 43 |
| ZnO/CPE | 1000−6000 | 0.3528 | this work |

[a]1-Methyl-3-octylimidazolium tetrafluoroborate = 1M3OIMZTFB, graphene = GR, molecularly imprinted polymer = MIP, boron doped diamond = BDD, ionic liquid (IL) 1-butyl-3-methylimidazolium hexafluorophosphate = ZIF-67/IL, screen printed electrodes = SPE, Prussian blue nanocubes = PBnc, pencil graphite electrode = PGE, molecularly imprinted polymer = MIP, polypyrrole = PPy, glassy carbon = GC.

**3.7. Antibacterial Activity.** The antibacterial activity of ZnO NPs toward *E. coli*, *S. aureus*, *P. aeruginosa*, and *S. pyogen* pathogenic bacteria were examined. The specific antibacterial activity mechanism of ZnO NPs is not yet very clear. However, a detailed antibacterial activity mechanism against pathogenic bacteria (genetic molecules) is summarized in Scheme 2 by modifying and adopting the picture from ref 44. In general, from the mechanism, ZnO NPs and their antibacterial activity have three major aspects: These are interaction between ZnO NPs and bacteria; release of $Zn^{2+}$; and generation of reactive oxide species (ROS). ZnO NPs possess positively charged characteristics in water suspensions. Hence, a good electrostatic attraction between ZnO NPs and bacteria due to the negatively charged nature of bacteria caused accumulation of NPs on it and changes the zeta potential. Such a change on bacteria caused the destruction of potassium channels on the bacterial cell membrane. In addition, $Zn^{2+}$ can combine with functional proteins, and this changes the cell membrane permeability.

A size range of 6.5 to 22.8 nm ZnO NPs was used for 50, 75, and 100 $\mu$g/mL concentrations, as shown in Table 5. From Table 5, the antibacterial activity of ZnO NPs against four pathogenic bacteria was elucidated by using ampicillin as a positive control. All of the activities were done using the disc diffusion test method, and their results are shown in Figure 8.

Synthesized ZnO NPs showed enhanced antibacterial activity against *S. pyogen* at higher concentrations (100 $\mu$g/mL). This is due to the fact that *S. pyogen* is a Gram-positive bacteria, so it is very simple to penetrate the cell wall of the bacteria and prevent the growth followed by the killing of the cell of this pathogenic bacteria. It is reported that Gram positive bacteria are surrounded by a peptidoglycan layer, and this could easily promote ZnO NP attack inside the cell wall. On the other hand, due to the presence of lipopolysaccharides in Gram-negative bacteria, there can be a counterattack of ZnO NPs.[45] However, *S. aureus* is also more exposed to ZnO NPs than *E. coli* and *P. aeruginosa* at all concentrations. In addition, ZnO NPs covered high zone inhibitions and were effective at higher concentrations, with a value of 100 $\mu$g/mL. It is noted that, as compared to all antibacterial activities, ampicillin (positive control) inhibits higher activity than ZnO NPs. All of the results are found to be in good agreement with previously reported work.[23,46−48] As can be confirmed from Table 5, the antibacterial activity of ZnO NPs toward *E. coli* and *P. aeruginosa* are found to be relatively low, and this in turn confirms that those bacteria strains contain a double cell membrane, which makes it difficult for the penetration of ions from ZnO MPs. As the dose of the bacteria is increased from 50 to 100 $\mu$g/mL, the antibacterial activity is also linearly increased. This is due to the fact that, as the dose of ZnO is increased, the excess amount of reactive oxygen species is increased, which enhances the killing of the cell of the targeted bacteria strains.

## 4. CONCLUSIONS

ZnO NPs were synthesized using *O. lamifolium* leaf extract, and this method is green, cost-effective, environmentally friendly, and simple. Precursor concentration, temperature, and time were optimized by using a simple I-optimal coordinate exchange RSM. The results indicated that zinc acetate has a primary effect on the synthesis of ZnO NPs. Thermal, surface, spectroscopic, and structural techniques were used to characterize the synthesized NPs. Structural and morphological results illustrated that the particle size of the prepared NPs was in the range between 6.5 and 22.8 nm. The electrochemical sensor activity of ZnO/CPE exhibited a linear regression in the range of 1 mM to 6 mM toward SMZ, which was effective with a LOD of 0.3528 $\mu$M. Furthermore, ZnO NPs demonstrated effective antibacterial inhibition at concentrations of 50, 75, and 100 $\mu$g/mL. Hence, the bacterial strain activity of ZnO NPs was effective for four different types of bacteria in the given zone of inhibition. In this regard, these findings have potential applications for diverse electrochemical activity for typical organic pollution detection and for any antimicrobial activities due to the intrinsic electrical con-


https://doi.org/10.1021/acsomega.3c02709
ACS Omega 2023, 8, 27344−27354

Scheme 2. Schematic Diagram of Antibacterial Activity and the Mechanism of ZnO NPs Toward *E. coli*, *S. aureus*, *P. aeruginosa*, and *S. pyogen*[44]

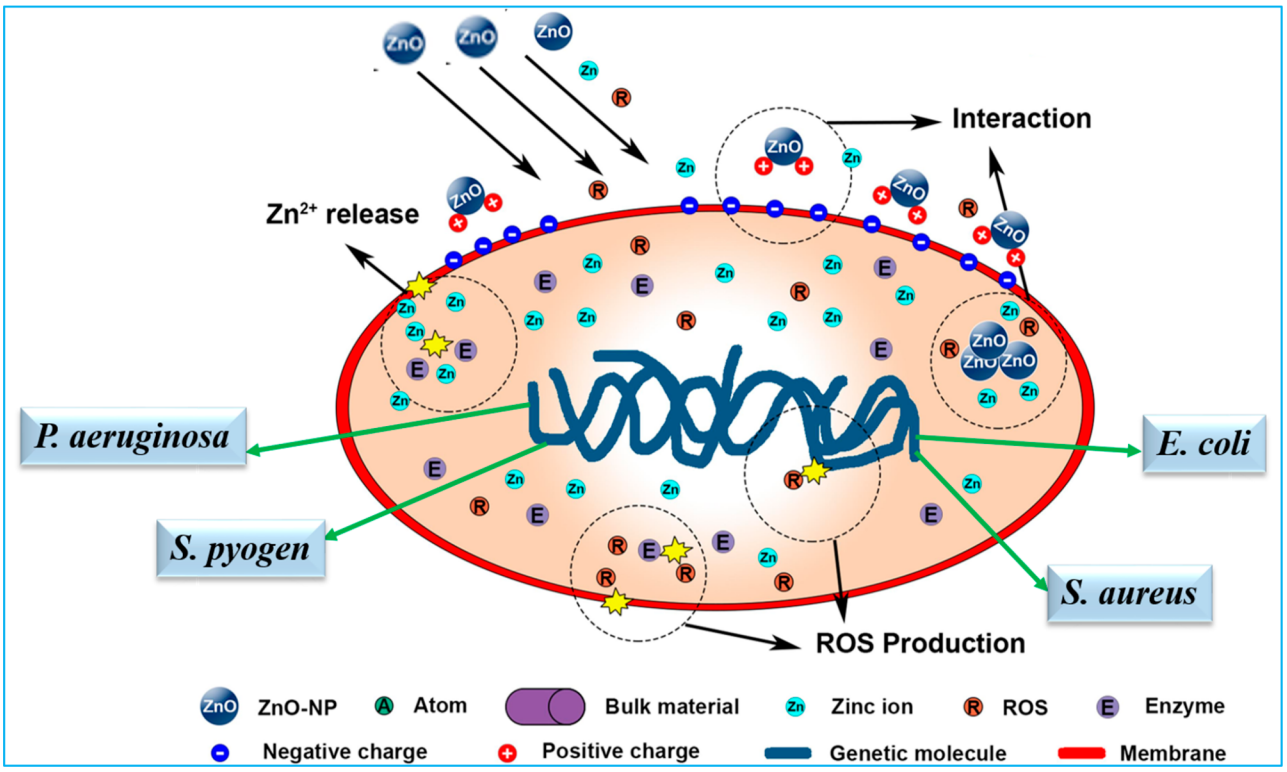


Table 5. Antibacterial Activity of ZnO NPs and Zone of Inhibition in mm

| compound concentration | *E. coli* (ATCC25922) | *S. aureus* (ATCC25923) | *P. aeruginosa* (ATCC27853) | *S. pyogen* (ATCC19615) |
|---|---|---|---|---|
| A = 50 μg/mL | 8 | 9 | 7.5 | 9 |
| B = 75 μg/mL | 9 | 10 | 9 | 10 |
| C = 100 μg/mL | 11 | 11.5 | 11 | 12 |
| ampicillin (positive control) | 12 | 12.5 | 12 | 13 |

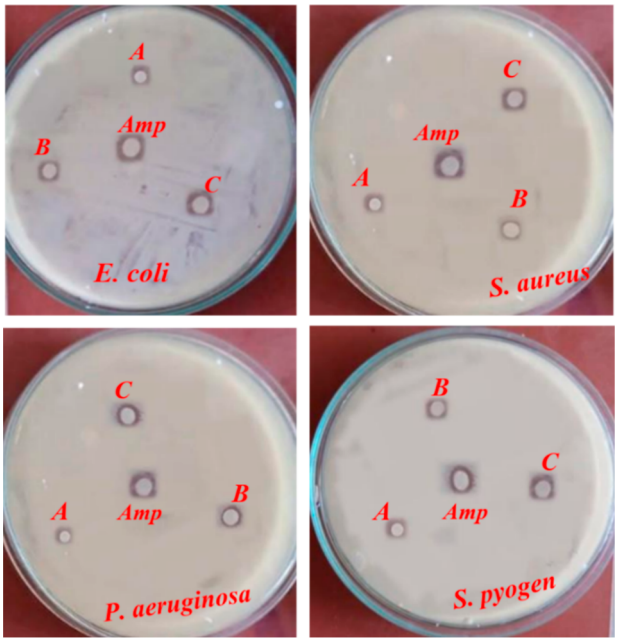


Figure 8. Antibacterial activity of ZnO NPs on *E. coli*, *S. aureus*, *P. aeruginosa*, and *S. pyogen* on disc (6 mm).

ductivity, environmental friendliness, and cost-effectivene nature of green synthesized ZnO NPs.

## AUTHOR INFORMATION


### Corresponding Author

**Yilkal Dessie** − *Department of Applied Chemistry, School of Applied Natural Science, Adama Science and Technology University, Adama 0000, Ethiopia*; orcid.org/0000-0001-7287-6499; Email: yilikaldessie@gmail.com

### Authors

**Eneyew Tilahun** − *Department of Applied Chemistry, School of Applied Natural Science, Adama Science and Technology University, Adama 0000, Ethiopia*

**Yeshaneh Adimasu** − *Department of Applied Biology, School of Applied Natural Science, Adama Science and Technology University, Adama 0000, Ethiopia*

Complete contact information is available at: https://pubs.acs.org/10.1021/acsomega.3c02709


### Notes

The authors declare no competing financial interest.



https://doi.org/10.1021/acsomega.3c02709
*ACS Omega* 2023, 8, 27344−27354

## ■ ACKNOWLEDGMENTS

The authors acknowledge Adama Science and Technology University for financial support of this work.

## ■ REFERENCES

(1) Ramesh, P.; Saravanan, K.; Manogar, P.; Johnson, J.; Vinoth, E.; Mayakannan, M. Green Synthesis and Characterization of Biocompatible Zinc Oxide Nanoparticles and Evaluation of Its Antibacterial Potential. *Sens. Bio-Sensing Res.* **2021**, *31*, 100399.

(2) Jadhav, N. A.; Singh, P. K.; Rhee, H. W.; Bhattacharya, B. Effect of Variation of Average Pore Size and Specific Surface Area of ZnO Electrode (WE) on Efficiency of Dye-Sensitized Solar Cells. *Nanoscale Res. Lett.* **2014**, *9* (1), 1−8.

(3) Selvanathan, V.; Aminuzzaman, M.; Tan, L. X.; Win, Y. F.; Guan Cheah, E. S.; Heng, M. H.; Tey, L. H.; Arullappan, S.; Algethami, N.; Alharthi, S. S.; Sultana, S.; Shahiduzzaman, M.; Abdullah, H.; Aktharuzzaman, M. Synthesis, Characterization, and Preliminary in Vitro Antibacterial Evaluation of ZnO Nanoparticles Derived from Soursop (Annona Muricata L.) Leaf Extract as a Green Reducing Agent. *J. Mater. Res. Technol.* **2022**, *20*, 2931−2941.

(4) Balasubramani, V.; Sureshkumar, S.; Rao, T. S.; Sridhar, T. M. Impedance Spectroscopy-Based Reduced Graphene Oxide-Incorporated ZnO Composite Sensor for H2S Investigations. *ACS Omega* **2019**, *4* (6), 9976−9982.

(5) Dönmez, S. Green Synthesis of Zinc Oxide Nanoparticles Using Zingiber Officinale Root Extract and Their Applications in Glucose Biosensor. *El-Cezeri J. Sci. Eng.* **2020**, *7* (3), 1191−1200.

(6) Kołodziejczak-Radzimska, A.; Markiewicz, E.; Jesionowski, T. Structural Characterisation of ZnO Particles Obtained by the Emulsion Precipitation Method. *J. Nanomater.* **2012**, *2012*, 1−9.

(7) Abel, S.; Tesfaye, J. L.; Shanmugam, R.; Dwarampudi, L. P.; Lamessa, G.; Nagaprasad, N.; Benti, M.; Krishnaraj, R. Green Synthesis and Characterizations of Zinc Oxide (ZnO) Nanoparticles Using Aqueous Leaf Extracts of Coffee (Coffea Arabica) and Its Application in Environmental Toxicity Reduction. *J. Nanomater.* **2021**, *2021*, 1−6.

(8) Naqvi, Q. ul A.; Kanwal, A.; Qaseem, S.; Naeem, M.; Ali, S. R.; Shaffique, M.; Maqbool, M. Size-Dependent Inhibition of Bacterial Growth by Chemically Engineered Spherical ZnO Nanoparticles. *J. Biol. Phys.* **2019**, *45* (2), 147−159.

(9) Fatimah, I.; Pradita, R. Y.; Nurfalinda, A. Plant Extract Mediated of ZnO Nanoparticles by Using Ethanol Extract of Mimosa Pudica Leaves and Coffee Powder. *Procedia Eng.* **2016**, *148*, 43−48.

(10) Doan Thi, T. U.; Nguyen, T. T.; Thi, Y. D.; Ta Thi, K. H.; Phan, B. T.; Pham, K. N. Green Synthesis of ZnO Nanoparticles Using Orange Fruit Peel Extract for Antibacterial Activities. *RSC Adv.* **2020**, *10* (40), 23899−23907.

(11) Guo, S.; Chen, X.; Ling, Y.; Wang, H.; Wei, X.; Pan, R.; Wang, P. Modification of a Carbon Paste Electrode with a ZnO@ZIF-8 Nanocomposite and Fabrication of a Highly Sensitive Electrochemical Sensor for Sulfamethoxazole Detection. *Int. J. Electrochem. Sci.* **2021**, *16*, 210950.

(12) Bekele, E. T.; Sintayehu, Y. D.; Murthy, H. C. A.; Shume, M. S.; Ayanie, G. T.; Turunesh, D. J.; Balachandran, R.; Tan, K. B.; Chan, K. Y.; Ghotekar, S.; Ravikumar, C. R. Synthesis of ZnO Nanoparticles Mediated by Natural Products of Acanthus Sennii Leaf Extract for Electrochemical Sensing and Photocatalytic Applications: A Comparative Study of Volume Ratios. *Chem. Pap.* **2022**, *76* (9), 5967−5983.

(13) Patil, V. B.; Ilager, D.; Tuwar, S. M.; Mondal, K.; Shetti, N. P. Nanostructured ZnO-Based Electrochemical Sensor with Anionic Surfactant for the Electroanalysis of Trimethoprim. *Bioengineering* **2022**, *9* (10), 521.

(14) T-Thienprasert, N. P.; T-Thienprasert, J.; Ruangtong, J.; Jaithon, T.; Srifah Huehne, P.; Piasai, O. Large Scale Synthesis of Green Synthesized Zinc Oxide Nanoparticles from Banana Peel Extracts and Their Inhibitory Effects against Colletotrichum Sp., Isolate KUFC 021, Causal Agent of Anthracnose on Dendrobium Orchid. *J. Nanomater.* **2021**, *2021*, 1−10.

(15) Darroudi, M.; Sabouri, Z.; Kazemi Oskuee, R.; Khorsand Zak, A.; Kargar, H.; Abd Hamid, M. H. N. Green Chemistry Approach for the Synthesis of ZnO Nanopowders and Their Cytotoxic Effects. *Ceram. Int.* **2014**, *40* (3), 4827−4831.

(16) Sabouri, Z.; Sabouri, S.; Moghaddas, S. S. T. H.; Mostafapour, A.; Gheibihayat, S. M.; Darroudi, M. Plant-Based Synthesis of Ag-Doped ZnO/MgO Nanocomposites Using Caccinia Macranthera Extract and Evaluation of Their Photocatalytic Activity, Cytotoxicity, and Potential Application as a Novel Sensor for Detection of $Pb^{2+}$ Ions. *Biomass Convers. Biorefinery* **2022**, DOI: 10.1007/s13399-022-02907-1.

(17) Sabouri, Z.; Sabouri, S.; Tabrizi Hafez Moghaddas, S. S.; Mostafapour, A.; Amiri, M. S.; Darroudi, M. Facile Green Synthesis of Ag-doped ZnO/CaO Nanocomposites with Caccinia Macranthera Seed Extract and Assessment of Their Cytotoxicity, Antibacterial, and Photocatalytic Activity. *Bioprocess Biosyst. Eng.* **2022**, *45* (11), 1799−1809.

(18) Saka, A.; Tesfaye, J. L.; Gudata, L.; Shanmugam, R.; Dwarampudi, L. P.; Nagaprasad, N.; Krishnaraj, R.; Rajeshkumar, S. Synthesis, Characterization, and Antibacterial Activity of ZnO Nanoparticles from Fresh Leaf Extracts of Apocynaceae, Carissa Spinarum L. (Hagamsa). *J. Nanomater.* **2022**, *2022*, 1−6.

(19) Xu, J.; Huang, Y.; Zhu, S.; Abbes, N.; Jing, X.; Zhang, L. A Review of the Green Synthesis of ZnO Nanoparticles Using Plant Extracts and Their Prospects for Application in Antibacterial Textiles. *J. Eng. Fiber. Fabr.* **2021**, *16*, 155892502110462.

(20) Alkasir, M.; Samadi, N.; Sabouri, Z.; Mardani, Z.; Khatami, M.; Darroudi, M. Evaluation Cytotoxicity Effects of Biosynthesized Zinc Oxide Nanoparticles Using Aqueous Linum Usitatissimum Extract and Investigation of Their Photocatalytic Activityackn. *Inorg. Chem. Commun.* **2020**, *119*, 108066.

(21) kermani, M.; Mostafapour, A.; Sabouri, Z.; Gheibihayat, S. M.; Darroudi, M. The Photocatalytic, Cytotoxicity, and Antibacterial Properties of Zinc Oxide Nanoparticles Synthesized Using Trigonella Foenum-Graecum L Extract. *Environ. Sci. Pollut. Res.* **2023**, *30* (7), 19313−19325.

(22) Faisal, S.; Jan, H.; Shah, S. A.; Shah, S.; Khan, A.; Akbar, M. T.; Rizwan, M.; Jan, F.; Wajidullah; Akhtar, N.; Khattak, A.; Syed, S. Green Synthesis of Zinc Oxide (ZnO) Nanoparticles Using Aqueous Fruit Extracts of Myristica Fragrans: Their Characterizations and Biological and Environmental Applications. *ACS Omega* **2021**, *6* (14), 9709−9722.

(23) Ravichandrika, K.; Kiranmayi, P.; Ravikumar, R. V. S. S. N. Synthesis, Characterization and Antibacterial Activity of ZnO Nanoparticles. *Int. J. Pharm. Pharm. Sci.* **2012**, *4* (4), 336−338.

(24) Abdelbaky, A. S.; Abd El-Mageed, T. A.; Babalghith, A. O.; Selim, S.; Mohamed, A. M. H. A. Green Synthesis and Characterization of ZnO Nanoparticles Using Pelargonium Odoratissimum (L.) Aqueous Leaf Extract and Their Antioxidant, Antibacterial and Anti-Inflammatory Activities. *Antioxidants* **2022**, *11* (8), 1444.

(25) Zewde, D.; Geremew, B. Biosynthesis of ZnO Nanoparticles Using Hagenia Abyssinica Leaf Extracts; Their Photocatalytic and Antibacterial Activities. *Environ. Pollut. Bioavailab.* **2022**, *34* (1), 224−235.

(26) Chaudhuri, S. K.; Malodia, L. Biosynthesis of Zinc Oxide Nanoparticles Using Leaf Extract of Calotropis Gigantea: Characterization and Its Evaluation on Tree Seedling Growth in Nursery Stage. *Appl. Nanosci.* **2017**, *7* (8), 501−512.

(27) Raja Ahmad, R. A.; Harun, Z.; Othman, M. H. D.; Basri, H.; Yunos, M. Z.; Ahmad, A.; Mohd Akhair, S. H.; Abd Rashid, A. Q.; Azhar, F. H.; Alias, S. S.; Ainuddin, A. R. Biosynthesis of Zinc Oxide Nanoparticles by Using Fruits Extracts of Ananas Comosus and Its Antibacterial Activity. *Malaysian J. Fundam. Appl. Sci.* **2019**, *15* (2), 268−273.

(28) Rahman, F.; Majed Patwary, M. A.; Bakar Siddique, M. A.; Bashar, M. S.; Haque, M. A.; Akter, B.; Rashid, R.; Haque, M. A.; Royhan Uddin, A. K. M. Green Synthesis of Zinc Oxide Nanoparticles



https://doi.org/10.1021/acsomega.3c02709
*ACS Omega* 2023, 8, 27344−27354

Using Cocos Nucifera Leaf Extract: Characterization, Antimicrobial, Antioxidant and Photocatalytic Activity. *R. Soc. Open Sci.* **2022**, *9* (11), DOI: 10.1098/rsos.220858.
(29) Gupta, M.; Tomar, R. S.; Kaushik, S.; Mishra, R. K.; Sharma, D. Effective Antimicrobial Activity of Green ZnO Nano Particles of Catharanthus Roseus. *Front. Microbiol.* **2018**, *9* (SEP), 1893.
(30) Kahsay, M. H. Synthesis and Characterization of ZnO Nanoparticles Using Aqueous Extract of Becium Grandiflorum for Antimicrobial Activity and Adsorption of Methylene Blue. *Appl. Water Sci.* **2021**, *11* (2), 45.
(31) Mandal, H.; Shyamal, S.; Hajra, P.; Samanta, B.; Fageria, P.; Pande, S.; Bhattacharya, C. Improved Photoelectrochemical Water Oxidation Using Wurtzite ZnO Semiconductors Synthesized through Simple Chemical Bath Reaction. *Electrochim. Acta* **2014**, *141*, 294−301.
(32) Suresh, J.; Pradheesh, G.; Alexramani, V.; Sundrarajan, M.; Hong, S. I. Green Synthesis and Characterization of Zinc Oxide Nanoparticle Using Insulin Plant (Costus Pictus D. Don) and Investigation of Its Antimicrobial as Well as Anticancer Activities. *Adv. Nat. Sci. Nanosci. Nanotechnol.* **2018**, *9* (1), 015008.
(33) Sabouri, Z.; Kazemi Oskuee, R.; Sabouri, S.; Tabrizi Hafez Moghaddas, S. S.; Samarghandian, S.; Sajid Abdulabbas, H.; Darroudi, M. Phytoextract-Mediated Synthesis of Ag-Doped ZnO-MgO-CaO Nanocomposite Using Ocimum Basilicum L Seeds Extract as a Highly Efficient Photocatalyst and Evaluation of Their Biological Effects. *Ceram. Int.* **2023**, *49* (12), 20989−20997.
(34) Sahoo, R.; Mundamajhi, A.; Das, S. K. Growth of ZnO Nanoparticles Prepared from Cost Effective Laboratory Grade ZnO Powder and Their Application in UV Photocatalytic Dye Decomposition. *J. Mater. Sci. Mater. Electron.* **2019**, *30* (5), 4541−4547.
(35) Pan, Y.; Zuo, J.; Hou, Z.; Huang, Y.; Huang, C. Preparation of Electrochemical Sensor Based on Zinc Oxide Nanoparticles for Simultaneous Determination of AA, DA, and UA. *Front. Chem.* **2020**, *8*, 1−7.
(36) Balasubramanian, P.; Settu, R.; Chen, S. M.; Chen, T. W. Voltammetric Sensing of Sulfamethoxazole Using a Glassy Carbon Electrode Modified with a Graphitic Carbon Nitride and Zinc Oxide Nanocomposite. *Microchim. Acta* **2018**, *185* (8), 396.
(37) Yue, X.; Li, Z.; Zhao, S. A New Electrochemical Sensor for Simultaneous Detection of Sulfamethoxazole and Trimethoprim Antibiotics Based on Graphene and ZnO Nanorods Modified Glassy Carbon Electrode. *Microchem. J.* **2020**, *159* (April), 105440.
(38) Salmanpour, S.; Khalilzadeh, M. A.; Karimi-Maleh, H.; Zareyeea, D. An Electrochemical Sensitive Sensor for Determining Sulfamethoxazole Using a Modified Electrode Based on Biosynthesized NiO Nanoparticles Paste Electrode. *Int. J. Electrochem. Sci.* **2019**, *14*, 9552−9561.
(39) Zhao, Y.; Yuan, F.; Quan, X.; Yu, H.; Chen, S.; Zhao, H.; Liu, Z.; Hilal, N. An Electrochemical Sensor for Selective Determination of Sulfamethoxazole in Surface Water Using a Molecularly Imprinted Polymer Modified BDD Electrode. *Anal. Methods* **2015**, *7* (6), 2693−2698.
(40) Shahsavari, M.; Tajik, S.; Sheikhshoaie, I.; Beitollahi, H. Fabrication of Nanostructure Electrochemical Sensor Based on the Carbon Paste Electrode (CPE) Modified With Ionic Liquid and Fe3O4/ZIF-67 for Electrocatalytic Sulfamethoxazole Detection. *Top. Catal.* **2022**, *65* (5−6), 577−586.
(41) Sgobbi, L. F.; Razzino, C. A.; Machado, S. A. S. A Disposable Electrochemical Sensor for Simultaneous Detection of Sulfamethoxazole and Trimethoprim Antibiotics in Urine Based on Multiwalled Nanotubes Decorated with Prussian Blue Nanocubes Modified Screen-Printed Electrode. *Electrochim. Acta* **2016**, *191*, 1010−1017.
(42) Özkorucuklu, S. P.; Şahin, Y.; Alsancak, G. Voltammetric Behaviour of Sulfamethoxazole on Electropolymerized- Molecularly Imprinted Overoxidized Polypyrrole. *Sensors* **2008**, *8* (12), 8463−8478.
(43) Ozkorucuklu, S. P.; Sahin, Y.; Alsancak, G. Determination of Sulfamethoxazole in Pharmaceutical Formulations by Flow Injection System/HPLC with Potentiometric Detection Using Polypyrrole Electrode. *J. Braz. Chem. Soc.* **2011**, *22* (11), 2171−2177.
(44) Li, Y.; Yang, Y.; Qing, Y.; Li, R.; Tang, X.; Guo, D.; Qin, Y. Enhancing ZnO-NP Antibacterial and Osteogenesis Properties in Orthopedic Applications: A Review. *Int. J. Nanomedicine* **2020**, *15*, 6247−6262.
(45) Lallo da Silva, B.; Abuçafy, M. P.; Berbel Manaia, E.; Oshiro Junior, J. A.; Chiari-Andréo, B. G.; Pietro, R. C. R.; Chiavacci, L. A. Relationship Between Structure And Antimicrobial Activity Of Zinc Oxide Nanoparticles: An Overview. *Int. J. Nanomedicine* **2019**, *14*, 9395−9410.
(46) Fuku, X.; Diallo, A.; Maaza, M. Nanoscaled Electrocatalytic Optically Modulated ZnO Nanoparticles through Green Process of Punica Granatum L. and Their Antibacterial Activities. *Int. J. Electrochem.* **2016**, *2016*, 1−10.
(47) Sikora, P.; Augustyniak, A.; Cendrowski, K.; Nawrotek, P.; Mijowska, E. Antimicrobial Activity of Al2O3, CuO, Fe3O4, and ZnO Nanoparticles in Scope of Their Further Application in Cement-Based Building Materials. *Nanomaterials* **2018**, *8* (4), 212.
(48) Bhuyan, T.; Mishra, K.; Khanuja, M.; Prasad, R.; Varma, A. Biosynthesis of Zinc Oxide Nanoparticles from Azadirachta Indica for Antibacterial and Photocatalytic Applications. *Mater. Sci. Semicond. Process.* **2015**, *32*, 55−61, DOI: 10.1016/j.mssp.2014.12.053.


https://doi.org/10.1021/acsomega.3c02709
*ACS Omega* 2023, 8, 27344−27354